Synthesis and Characterization of Novel Nano-carbon Mixture from Dabai (*Canarium odontophyllum*) Nutshell

Anthonette Anak James,[a] Md Rezaur Rahman,[a,*] Durul Huda,[b] Faisal M. Aqlan,[c] Mohammed Mahbubul Matin[f], Muhammad Khusairy Bin Bakri,[a] Kuok King Kuok,[d] and Mohammed Muzibur Rahman [e]

The nanocarbon-based mixture was shown to be an effective adsorbent for removing dyes and heavy metals from wastewater *via* adsorption. The goal of this research was to prepare and investigate the properties of a bio-carbon mixture made from Dabai (*Canarium odontophyllum*) nutshell with the addition of titanium dioxide (TiO_2) and montmorillonite (MMT) clay. Fourier transform infrared (FTIR) spectroscopy was used to determine the functional groups of raw carbon and potassium hydroxide (KOH)-activated carbon (AC). The FTIR analysis of the active carbon revealed that the active carbon had more surface chemistry than the non-AC. Scanning electron microscopy (SEM) analysis was used to compare the raw and AC morphologies and the developed nanocarbon. The results were confirmed using energy dispersive X-ray (EDX) analysis to verify the elements in the studied sample. The SEM analysis revealed that the structure of both the carbon samples was irregular, granular, and porous. BET analysis showed that nano-activated carbon had higher surface area compared to activated carbon itself. Response surface methodology (RSM) was used in Design-Expert 13.0 software for the sample composition development to achieve the best performance of the developed nanocarbon as an adsorbent.

DOI: 10.15376/biores.17.3.4452-4469

Keywords: Activated carbon; Adsorption; Response surface methodology; Nanocarbon

Contact information: a: Faculty of Engineering, Universiti Malaysia Sarawak Jalan Datuk Mohammad Musa 94300, Kota Samarahan, Sarawak, Malaysia; b: Department of Mechanical Engineering and Product Design Engineering, Swinburne University of Technology, 3122, Hawthorn, Victoria, Australia; c Department of Chemistry, College of Sciences, University of Jeddah, 21589 Jeddah, P.O. Box 80327, Saudi Arabia.; d: Faculty of Engineering, Computing, and Science, Swinburne University of Technology Sarawak Campus, 93400, Kuching, Sarawak, Malaysia; e: Department of Chemistry & Center of Excellence for Advanced Materials Research (CEAMR), Faculty of Science, King Abdulaziz University, Jeddah 21589, P.O. Box 80203, Saudi Arabia; f: Bioorganic and Medicinal Chemistry Laboratory, Department of Chemistry, Faculty of Science, University of Chittagong, Chittagong, 4331, Bangladesh
**Corresponding author: rmrezaur@unimas.my*

INTRODUCTION

Activated carbon products made from plant resources are among the most important adsorbents in the wastewater treatment industry. Due to the abundance of biomass resources and simple production routes, several studies on the synthesis of carbonaceous materials from biomass have been conducted (Varma 2019; Son *et al*. 2021). These two factors have been identified as two key contributors to the rapid development of carbonaceous materials. Many recent studies have focused on low-cost and sustainable carbonaceous materials that are produced from industrial by-products or agricultural waste, as conventional adsorbents have some limitations in terms of cost and regeneration (Gisi

et al. 2016; Karoui *et al*. 2019; Maguana *et al*. 2019; Chikri *et al*. 2020). This problem has prompted researchers to seek natural non-conventional adsorbents due to their renewability, sustainability, and biocompatibility in treating industrial effluent. The production of carbonaceous materials from biomass has several advantages, including cost-effectiveness, sustainability, and environmental friendliness (Zaman *et al*. 2017; Wataniyakul *et al*. 2018). Saleem *et al.* (2019) and Ahmad and Azam (2019) stated that activated carbonaceous material has an excellent pore structure with a large surface area and good adsorption ability in removing organic and inorganic contaminants from wastewater.

Canarium odontophyllum, also known as Dabai, has been recognized as a possible raw material for activated carbon (AC) production. Dabai, a seasonal fruit, is abundantly found in tropical forests in East Malaysia, specifically in Sibu, Sarawak. A rough and woody endocarp of Dabai seed contains edible cotyledon inside, and the physical traits of this nutshell mimic those of a palm kernel shell. Studies related to Dabai nutshell are relatively new, as it has been discovered that Dabai has strong adsorbent properties. According to Kuang *et al*. (2020) and Srivatsav *et al.* (2020), the functional groups present on the surface of Dabai nutshell have a vital role in wastewater adsorption due to their effectiveness in adsorbing multiple ranges of pollutants, such as dyes, hazardous materials, and heavy metals. Chikri *et al*. (2020) found that using acid and alkali solutions during the pre-treatment of AC-based lignocellulosic materials improved its adsorption properties. However, there is still a scarcity of information on Dabai nutshell AC for wastewater treatment with titanium dioxide (TiO_2) and montmorillonite (MMT) nano clay. The titanium dioxide (TiO_2) has photocatalytic activity which results in thin coatings exhibiting self-cleaning and disinfecting properties under exposure to ultraviolet radiation

This study aimed to develop a nanocarbon mixture from Dabai nutshells through a pyrolysis process with potassium hydroxide (KOH) solution to activate the micropores and mesopores of AC, which is one of the crucial factors in facilitating the adsorption reaction. In this study, two types of carbonaceous materials were prepared, including non-AC and AC. Finally, nano-sized particles were prepared using milling AC and nano-AC along with TiO_2 and montmorillonite (Khui *et al.* 2020). The manufactured mixture was compatible with each other, and it provides a larger surface area due to the montmorillonite (MMT) nano-clay which has easily helped to bind the pollutants from wastewater. The study also employed Fourier transform infrared spectroscopy (FTIR), scanning electron microscopy (SEM), and energy-dispersive X-ray spectroscopy (EDX) to evaluate the morphological, chemical, and physical properties, as well as the composition of the developed nanocarbon mixture. In addition, critical analysis and comparisons were performed to validate the performance of the developed nanocarbon against the available results.

EXPERIMENTAL

Materials

The titanium (IV) oxide (CAS Number: 14363-67-7), MMT K10 (CAS Number 1318-93-0), and zinc oxide (CAS Number 1314-13-2) were obtained from Sigma-Aldrich Sdn (Petaling Jaya, Malaysia). The Dabai nutshell (*C. Odontophyllum*) was obtained from Sibu, Sarawak, Malaysia.

Methods

Sample preparation

The Dabai seed was collected from an orchard located in Sibu, Sarawak, Malaysia during the seasonal period. The Dabai nutshell was air-dried and stored in an airtight compartment. Seeds were crushed with a pestle and mortar to separate the kernel from the nutshell. They were then soaked in an acetone solution to remove impurities and cleaned with deionized water. The sample was placed in an oven at 110 °C for 24 h to dry. After drying, the sample was crushed and sieved (after sieving, the particle size was less than 0.036 mm) once more to obtain small particles that would increase the surface interaction during activation.

Chemical activation of the prepared sample

Twenty grams of ground Dabai shell were treated and activated using 100 mL of KOH in an auto-shaker at 140 rpm for 24 h. After completing the sample activation, the sample was washed thoroughly with deionized water until the pH 7. After obtaining desired values of pH 7, the sample was placed in the oven to dry at 80 °C for 12 h. The sample was spread on a plate to ensure even heat distribution and to eliminate variable hotpots during the drying process

Carbonization of the sample

The carbonization process was performed using an LT Furnace (Selangor, Malaysia). The dried treated Dabai particle was then transferred into a ceramic bowl and wrapped in aluminum foil and a layer of clay before it was placed in the LT Furnace for carbonization. During the carbonization step, the temperature was ramped from room temperature to 200 ℃, followed by 400 ℃ at a heating rate of 10 ℃/min. At 400 ℃, the temperature was maintained for 1 h for the carbonization process to occur. Next, the furnace was cooled at 6.16 ℃/min until it reached room temperature. The sample was left overnight and retrieved from a furnace the next day. The fine biocarbon was obtained after completing the carbonization process. Next, it was collected and sieved using a 200 μm sieve to reduce the fine biocarbon (or fine biochar) and assist the ball milling process.

Nano-carbon preparation by the ball milling process

To further assist the ball milling process, the sieved biocarbon (or biochar) obtained was further ground using a grinder for approximately 5 to 10 min at a speed ranging between 18,000 and 20,000 rpm. The ground biocarbon was added into the cylindrical compartment of the ball mill (approximately 55% of the capacity). Twenty small-size stainless-steel ball of 0.5 g each were used to transform the biochar into a nano size. The biochar was milled for 30 h, and the sample was extracted for testing periodically at an interval of time to ensure it reached to the 50 to 120 nm.

Preparation of the nano AC mixture

The Dabai-based activated nano-carbon, the TiO_2, and the MMT were mixed according to the composition results in Table 1 to prepare the nanocarbon mixture. The composition results were prepared using Design-Expert 13.0 software (StatEase, Minneapolis, MN, USA).

FTIR Analysis

An IRAffinity-1 FTIR spectrophotometer (Shimadzu, Kyoto, Japan) was used to examine the functional groups and structures of the molecular bond by analyzing the IR spectrum bands between 4000 and 400 cm^{-1}. Approximately 0.1 to 1.0% of the sample were mixed with 200 to 250 mg of dry powder KBr in a small agate pestle to create a sample pellet for FTIR spectroscopy. Then, the mixture was pelletized and taken into the sample holder inside the spectroscopy. The FTIR spectrum results were analyzed using the ASTM E1252-98 (2021) and ASTM E168-16 (2016) standards.

Table 1. Experimental Factors

Std	Run	Factor 1 A: KOH-AC (wt%)	Factor 2 B: TiO_2 (wt%)	Factor 3 C: Clay (wt%)
16	1	3.00	0.55	1.25
3	2	1.00	1.00	0.50
2	3	5.00	0.10	0.50
15	4	3.00	0.55	1.25
1	5	1.00	0.10	0.50
10	6	3.00	1.31	1.25
4	7	5.00	1.00	0.50
8	8	5.00	1.00	2.00
13	9	3.00	0.55	1.25
9	10	6.36	0.55	1.25
6	11	5.00	0.10	2.00
11	12	3.00	0.55	2.51
5	13	3.00	0.55	1.25
7	14	1.00	1.00	2.00
14	15	3.00	0.55	1.25
17	16	3.00	0.55	1.25
12	17	1.00	0.10	2.00

SEM Analysis

A Hitachi analytical tabletop SEM (benchtop) (TM-3030, Hitachi High Technologies, Mannheim, Germany) was used to examine the morphological image data of the samples, particularly the porosity. The samples were positioned on aluminum stubs and fine-coated with a JFC-1600 auto fine coater (JEOL, Tokyo, Japan). The images of the nanocarbon surface were collected using a field emission gun with 5 and 15 kV voltage values. This procedure was carried out according to the ASTM E2015-04 standard (2014).

EDX Analysis

The EDX analysis was used to determine the elementary composition of materials in the sample.

BET Surface are of Activated Carbon (AC) and Nano Activated Carbon (NAC)

The BET surface area analysis was conducted according to the ASTM D6556-14 (2014) standard. The degassing temperature was set at 130 °C for 3 h. The test was repeated numerous times for each sample and the most representative results were selected.

RESULTS AND DISCUSSION

FTIR Analysis of the Raw Carbon and the KOH-AC

The main functional groups in the Dabai nutshell raw carbon were determined based on the O−H and C−H stretching bands, as depicted in Fig. 1. A strong O−H stretching band was observed at the peaks of 3591.5, 3363.9, and 3169.0 cm^{-1}. This finding is supported by the presence of the O−H functional group in raw corncob carbon, as mentioned by Feng *et al.* (2020). Zheng *et al.* (2018) investigated the microcrystalline in biomass and discovered that the band becomes less intense as the reformation of intermolecular hydrogen bonds between free hydroxyl and water molecules increases. This is due to the breakdown of intermolecular and intramolecular hydrogen bonds in the main chain of cellulose during the physical process. In addition, the C−H band was visible at peak intensities of 2897.1 and 2735.1 cm^{-1}. This band is defined by Zheng *et al.* (2018) as aliphatic moieties of symmetric and asymmetric C−H groups in polysaccharides. The peak intensity at 2897.1 cm^{-1} showed the presence of methylene with C−H stretching in the non-activated sample. Salim *et al.* (2021) also specified a similar band observed in the FTIR result of *Leucaena leucocephala* bark, which indicates the aromatic methoxyl group of lignin, methylene, and methyl groups. Besides, isothiocyanate ions are detected with the appearance of peaks at 2173.8, 2123.6, and 2044.5 cm^{-1}. The aryl-alkyl ether functional group was found at the peak of 1269.2 cm^{-1}, which as attributed to the C−O−C stretching motion. Aside from that, the presence of the C−H aromatic hydrogen linkage was also detected at the absorbance bands of 869.9 and 823.6 cm^{-1} (Fig. 1).

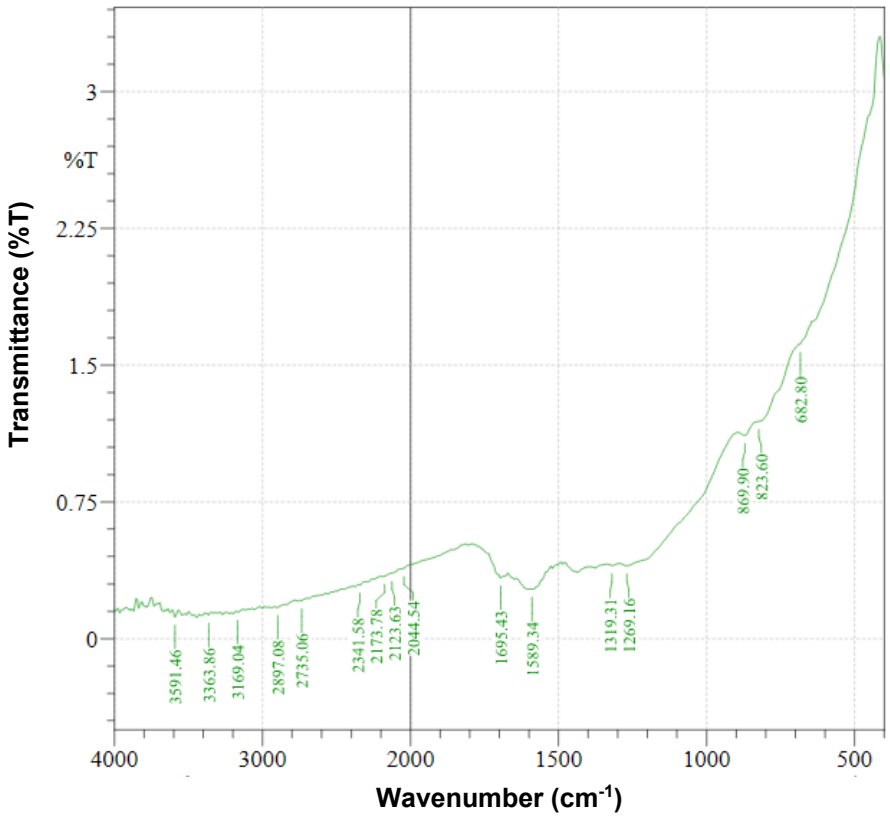

Fig. 1. IR spectra of the Dabai based raw carbon

The presence of a peak at 1589.3 cm^{-1} referred to the C=C stretching in an aromatic skeletal mode of lignin. This peak was slightly reduced to 1577.8 cm^{-1} after undergoing chemical activation with KOH. The degradation of lignin, which involves aryl ether bonding, would initiate the formation of phenolic components, particularly ferulic acid and *p*-coumaric acid (Janusz *et al*. 2017; Li and Wilkins 2020). The decrease of lignin provides a good structural effect to the AC as it can increase the structure porosity of the sample (Darmawan *et al*. 2016; Poursorkhabi *et al*. 2020). The appearance of functional groups such as O−H, C=O, C−O−C, C−O, and C−H alkyl and aromatic identified the presence of polysaccharides in the raw carbon before the chemical activation (Darmawan *et al*. 2016). Compared to the IR spectra in Fig. 1, the IR spectra in Fig. 2 was flatter, ranging from 3000 to 1000 cm^{-1}. Unlike the Dabai raw carbon, the FTIR results of the Dabai AC displayed an apparent decrease in the peak intensity, indicating that the samples lost functional groups during the activation process volatilization. As a result, the Dabai activated carbon had a weak band, and some cellulose remained in the sample. The peak intensities between 1600 and 1700 cm^{-1} referred to the functional carboxylic acid group in the raw and carbonized materials. This peak can be found at an absorbance band of 1764.9 cm^{-1} in Fig. 2. However, because carbonized materials have an alkali pH, the band intensity was reduced in the carbonized sample. This is supported by the findings of Mistar *et al.* (2020), where a reduction in the peak intensities in palm oil trunk biochar compared to the raw sample was found. The effect of the pre-treatment technique on the lignocellulosic material resulted in the formation of the carboxylic acid functional group. The peak at 2870.1 cm^{-1} represented the methylene functional group (C−H stretching). Four peaks distinguished from the O−H stretching were detected at 3782.4, 3489.2, 3280.9, and 3170.1 cm^{-1}. According to Bernal *et al.* (2018), the functional groups detected in the FTIR spectra are formed by the reaction of heteroatoms such as hydrogen, oxygen, and nitrogen with the carbon matrix.

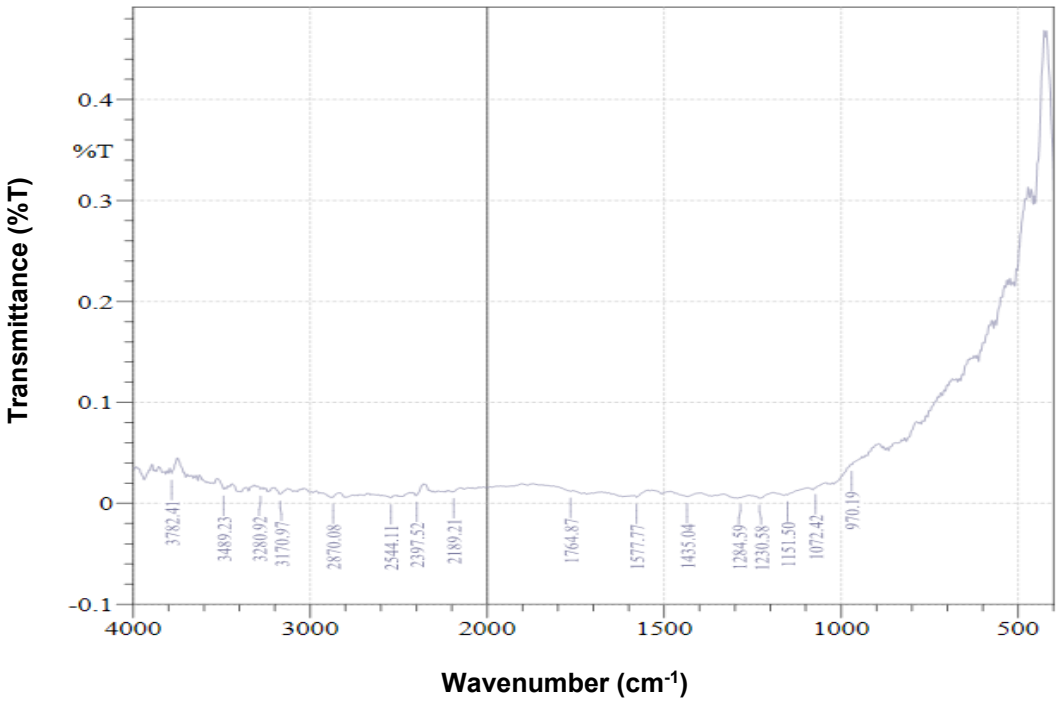

Fig. 2. IR spectra of the KOH-AC

FTIR Analysis of the AC/TiO_2/MMT Mixture

Figure 3 shows the FTIR results for the developed AC/TiO_2/MMT mixture. The adsorption band at 1600.9 cm^{-1} indicates the C=C stretching of the conjugated and cyclic alkene of mixture. The peak intensity at 1203.6 cm^{-1} shows the adsorption peak of a solid C−O stretching band of alkyl aryl ether, while the peak at 1035.8 cm^{-1} distinguished a strong S=O stretching in AC/TiO_2/MMT mixture before the adsorption process. According to Chobchun *et al.* (2020) and Kusiak-Nejman *et al.* (2018), the peak between 1038 and 1060 cm^{-1} represents C and Ti-O electron affinity, indicating the incorporation of carbon into TiO_2.

The peak at 634.58 cm^{-1} refers to the C−Cl stretching band of the halo compound. The appearance of peak intensities at 565.14 and 536.21 cm^{-1} in Fig. 7 represents the Si−O stretching variation bond of the MMT nanofiller (Mohammed *et al*. 2020). Such peaks also have been observed in the study of palm oil mill effluent (POME) treatment using developed silica membrane and poly(L-lactic acid)-poly(ethylene glycol) conducted by Kamil *et al.* (2020). The presence of these peaks provides a good adhesion interaction within the mixture. Arjmandi *et al.* (2016) and Li *et al.* (2017) reported that MMT has several uniform polar sites on its structure that indicate the content of electron density along with the interlayer spaces and their surfaces. As stated by Kuang *et al.* (2020) and Ahrouch *et al.* (2019), the addition of MMT clay has little effect on the chemical composition, but it lowers the adsorption peak of AC. This is supported by the findings of Arjmandi *et al.* (2016), which reported that the chemical structure of MMT clay with mixture does not change because no new functional groups are observed.

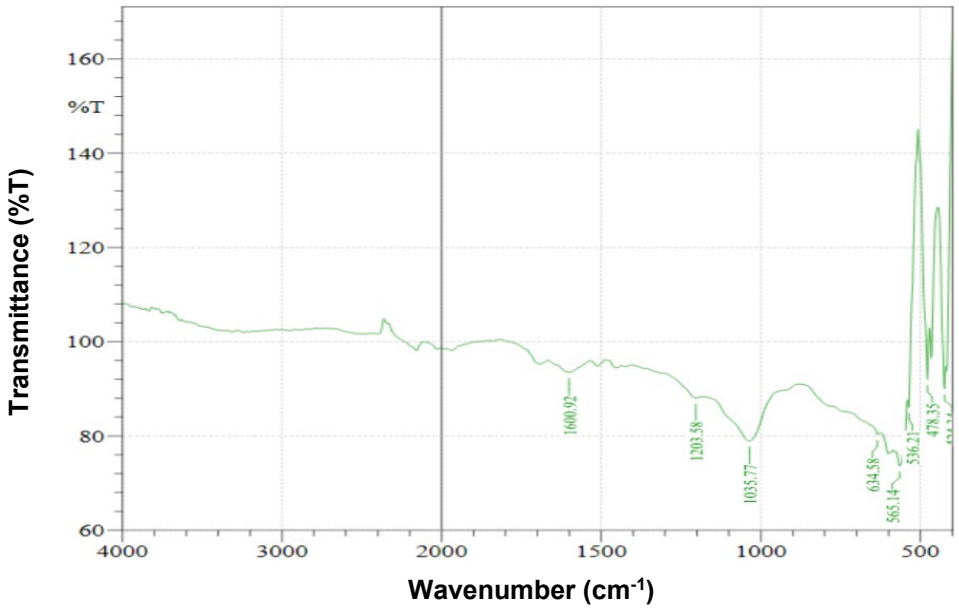

Fig. 3. IR spectra of the AC/TiO_2/MMT mixture before adsorption

Morphological Analysis of the Raw Carbon and the AC

The samples were analyzed by SEM to observe and visualize the surface texture of both the non-activated and the KOH-activated Dabai based carbon. Figures 4a and 4b show the surface morphologies of the non-activated and AC at 80× magnification, while Figs. 4c

and 4d show the surface morphologies at 1,000× magnification. Based on the observations, Fig. 4a offers multiple microfibrils with an irregular rod-like structure slightly more prominent than in Fig. 4b. The compact, rigid structure of the microfibrils particle exhibit an intuitive reduction into loosened open-pore width particles of roughly 140 to 80 µm, as illustrated in Fig. 4b. Based on Karinkanta *et al.* (2018) and Phanthong *et al*. (2018), this is due to the milling process where the reduction of size can be achieved with some split open on the structure, which degraded into small particles resulting in an increasing number of particulates (Fig. 4a). Zheng *et al.* (2018) observed the breakage and agglomeration in microcrystalline carbon particles during the mechanical grinding process, where individual carbon particles began to aggregate. Over milling may also initiate compact globular fragments of carbon exhibited granular texture, as shown by the red circle in Fig. 4b.

Figures 4c and 4d show the porous structure of the sample, distinguishing the general characteristics of the carbonaceous materials. By comparing these two figures, the size of the pores in Fig. 4d is much bigger, particularly between 6 and 8 µm. On the other hand, Fig. 4c shows pores in the size range of 3 to 4 µm. The activation process performed on Dabai nutshell-based carbon is expected to improve the porosity of AC. Heidarinejad *et al*. (2020) observed the porosity size of the AC's influence on the adsorption capacity of the sample. Mu'aza *et al.* (2017) and Gao *et al*. (2020) found that different types of the precursors, such as activating agents, would exhibit other characteristic behaviors for pores size, surface area, and distribution of particles. Due to the activation, the surface area was increased compared to non-activated Dabai nutshell-based carbon for enhancing the absorption capacity. This has been supported by Min *et al*. (2017), who found that some AC has poor porous structure due to the blocking effect of activating agents on the surface. According to Chowdhury *et al.* (2013), when the biomass materials used have indistinctive porosity, causing the alkaline dehydrating agents to be unable to penetrate the raw materials, which explains the poor porosity of the KOH-AC.

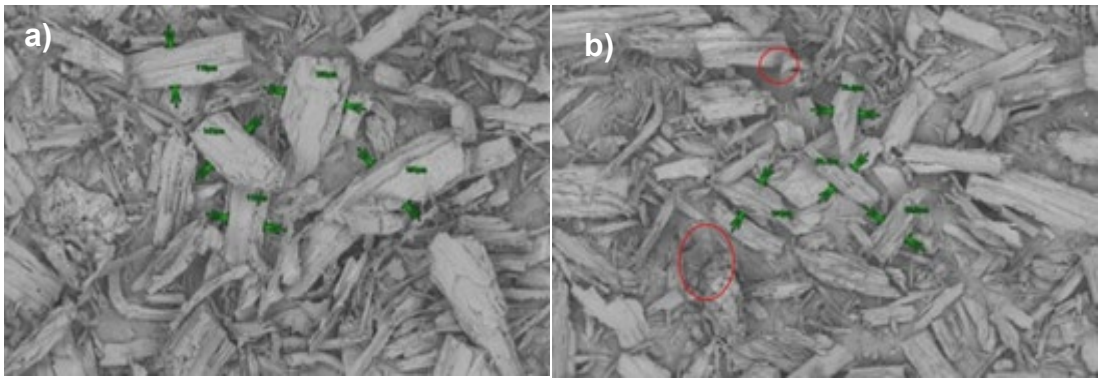

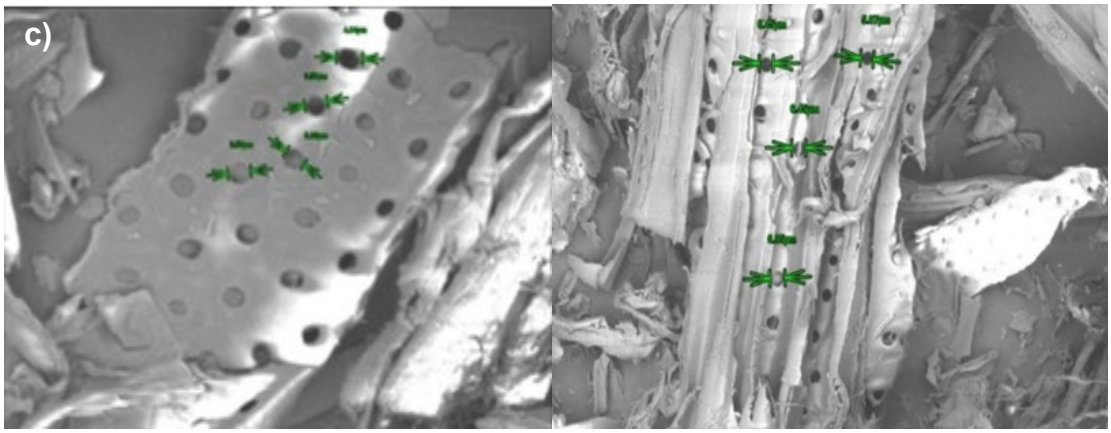

Fig. 4. Morphological images of the a) raw carbon (80× magnification), b) KOH-AC (80× magnification), c) raw carbon (1,500× magnification), and d) KOH-AC (1,500× magnification)

The activating agent KOH is used to activate both carbon micropores and mesopores. According to Deng *et al*. (2016), a mixture of three components (cellulose, lignin, and hemicellulose) initiates three-dimensional structures such as the porous structure of macropores, mesopores, and micropores as the amount of lignin present is less than 50%. The choice of KOH concentration for the activation process is crucial because it influences the formation of micropores in the internal void of KOH-AC (Yang *et al*. 2017). Yang *et al.* (2017) added that when the concentration of KOH is too high, it destroys the micropores, which causes them to grow in size. Though they would be too small to show up in these images, it is expected that the internal structure of KOH-AC formed numerous micropores and mesopores, which can increase the adsorption of contaminants from POME. This structure is similar to the result observed by Taoufik *et al*. (2019) in their research related to AC-TiO_2 for emerging pollutants removal.

Morphological Analysis of the AC/TiO_2/MMT Clay Mixture

The morphology of the developed powder is an essential critical characteristic that demonstrates how adsorption activity influences their application in wastewater treatment. Figures 5a and 5b show the SEM images of the sample 13 and sample 17 mixture, respectively, at 500× magnification, while Fig. 5c and 5d depict the images at 1,000× magnification. The distribution of the AC/TiO_2/MMT clay in sample 13 (Fig. 5a) was uneven because the AC content was much higher than the TiO_2 and MMT clay, as illustrated in Table 2. The SEM image of Fig. 5b with ratio 1:1:2 AC/TiO_2/MMT clay mixture shows an even composition distribution. The AC particles had an irregular rod-like shape, the MMT clay particles had larger white flakes, and the TiO_2 particles had smaller white fragments. Based on Djellabi *et al.* (2019) and Matteis *et al.* (2020), TiO_2 is easily trapped on the rough and homogeneous surface of the AC. This statement is supported by Fig. 5c, which illustrates some of the TiO_2 white flakes found on the surface of the AC. The findings support the FTIR analysis results for the powder in Fig. 5, where the attachment of TiO_2 on the AC rendered them unidentifiable by FTIR.

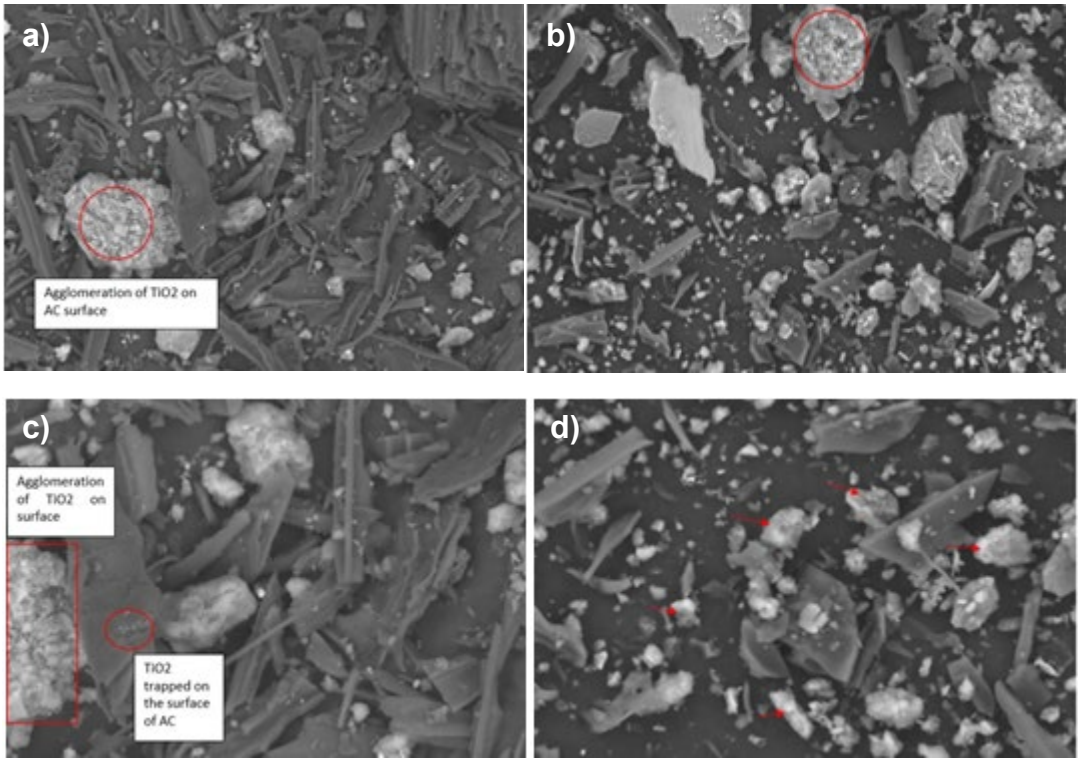

Fig. 5. Morphological images of sample a) 13 raw mixture (500× magnification), b) 17 raw mixture (500× magnification), c) 13 raw mixture (1,000× magnification), and d) 17 raw mixture (1,000× magnification)

Figures 5a and 5b show the roughened surfaces caused by the aggregation of the TiO_2 deposition on the surface due to poor dispersion of the particles. This finding was confirmed by Murugadoss *et al.* (2020), who discovered that TiO_2 agglomeration occurs due to suspended sample preparation influenced by time. The small uniform aggregation of TiO_2 and MMT clay dispersion in Fig. 5d provides more reactive sites than large, agglomerated particles, such as in Fig. 5e. Therefore, to create an effective non-conventional mixture, excellent dispersion of TiO_2 and MMT compositions is required over the sample, as uneven distribution may reduce the practical treatment ability (Keane 2013).

Table 2. Composition of the AC/TiO_2/ MMT Clay Mixture

Sample No.	AC (g)	TiO_2 (g)	MMT Clay (g)
Sample 13	6.36359	0.55	1.23
Sample 17	1	1	2

The EDX diffraction was correlated with the SEM analysis. The peaks of the element composition present in the AC/TiO_2/MMT clay mixture samples 13 and 17 are depicted in Figs. 6 and 7.

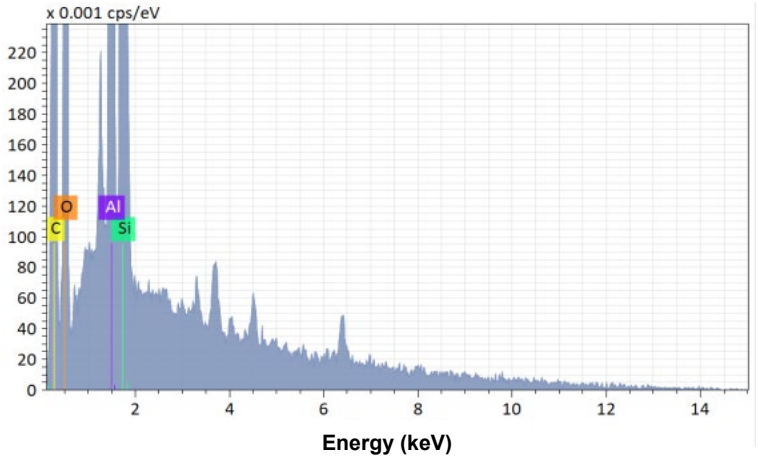

Fig. 6. EDX diffraction spectra with its element compositions of sample 13 (raw)

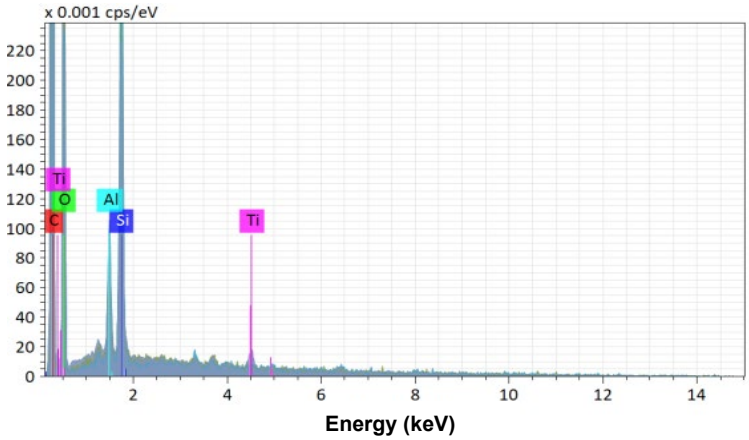

Fig. 7. EDX diffraction spectra with its element compositions of sample 17 (raw)

Based on the EDX spectrum presented by the graphs, the higher atomic percentage of elements was dominated by carbon (C) and oxygen (O). This illustrates that C and O are the main components of carbonaceous material. The C percentages for Tables 3 and 4 were 65.7% and 67.4%, while the O percentages were 27.1% and 28.7%, respectively. The findings concluded that the C and O contents in both samples were nearly identical, with a difference of 1% to 2%.

Table 3. EDX Composition of Sample 13 (raw)

Element	Mass (%)	Atom (%)	Abs. error (%) (σ)	Rel. error (%) (σ)
C	65.7268	73.6968	7.6456	11.6323
O	27.1276	22.8345	3.5370	13.0384
Si	4.9935	2.3945	0.2362	4.7296
Al	2.1522	1.0742	0.1287	5.9818

Table 4. EDX Composition of Sample 17 (raw)

Element	Mass (%)	Atom (%)	Abs. error (%) (σ)	Rel. error (%) (σ)
C	67.4021	74.4361	7.8577	11.6579
O	28.7240	23.8139	3.8400	13.3686
Si	2.7368	1.2926	0.1438	5.2531
Al	0.6628	0.3263	0.0606	9.1225
Ti	0.4733	0.1311	0.0466	9.8478

Analysis of the Brunauer-Emmett-Teller (BET) Surface Area

The Brunauer-Emmett-Teller (BET) test was conducted to evaluate the specific surface area of activated carbon after the milling process using nitrogen gas adsorption method at 77 K by Autosorb iQ Any Gas (AG) sorption. The specific surface area with a unit of m^2/g shows the porosity, shape, distribution of pore size, and roughness of the activated carbon (Amador and Martin 2016). According to the findings, Table 5 shows that the specific surface area for prepared activated carbon was 5.09 m^2/g, whereas the nano activated carbon was 25.8 m^2/g. This indicates that the ball milling method successfully reduced the particle size to nano scale (Khairulzaim *et al.* 2021; Inderan *et al.* 2014). The initial size was influenced by the pyrolysis process during activation and other factors such as nitrogen gas flow rate, temperature, and time (Quan *et al.* 2019; Zhang *et al.* 2019; Zuo *et al.* 2018). It was reflected on the SEM analysis, which shows a reduction in particle and pore sizes. The activation temperature promotes the formation of pore structures (Chen *et al.* 2018). Moreover, when the activation temperature reaches a certain point, the adsorption capacity of activated carbon was reduced due to the over-activated process. Figures 8, 9 and 10 represent the trend of the surface area of activated and nano activated carbon. Figure 8 revealed that the surface area increased with increases of the time for both activated and nano activated carbon. The adsorption capabilities of both activated carbons were shown in Figs. 9 and 10, respectively (Khui *et al.* 2020).

Table 5. Specific Surface Area (m^2/g) of Activated Carbon (AC) and Nanoactivated Carbon (NAC)

Carbon	Surface area (m^2/g)
Activated carbon (AC)	5.093
Nano-activated carbon (NAC)	25.779

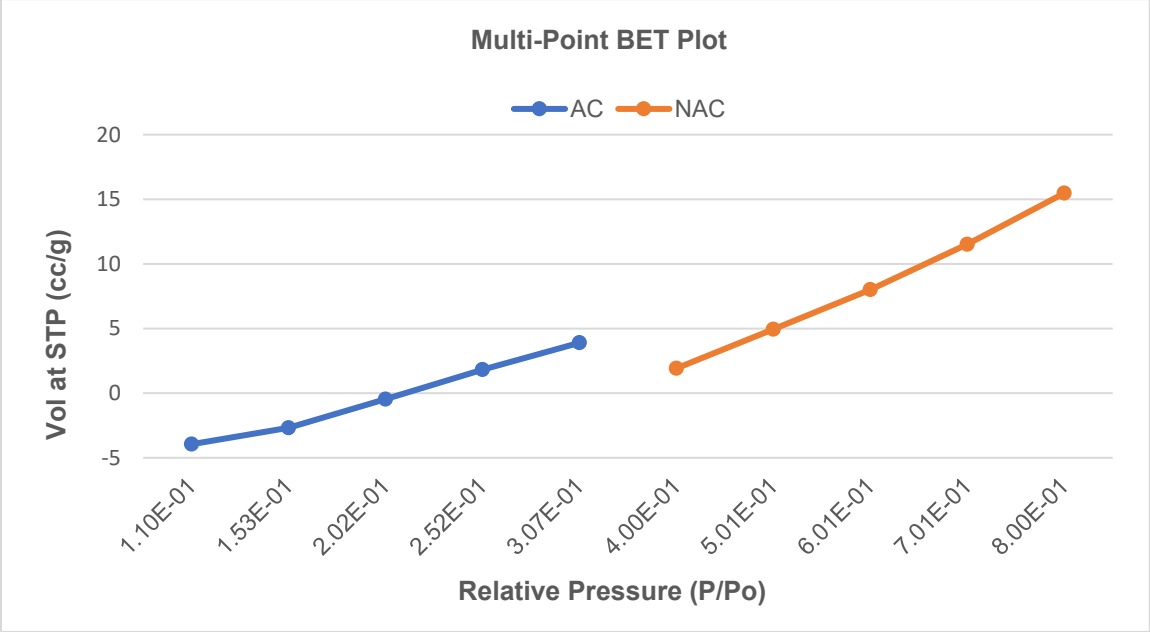

Fig. 8. Multi-Point BET plot for activated carbon and nano-activated carbon

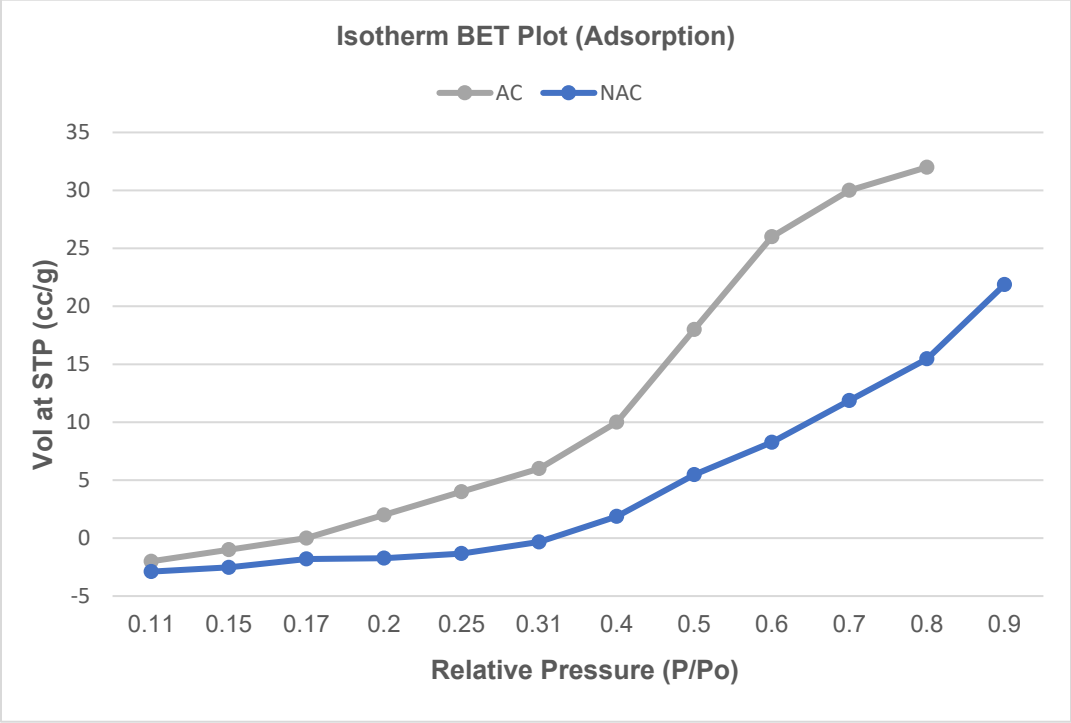

Fig. 9. Isotherm BET plot (adsorption) of activated and nano-activated carbon

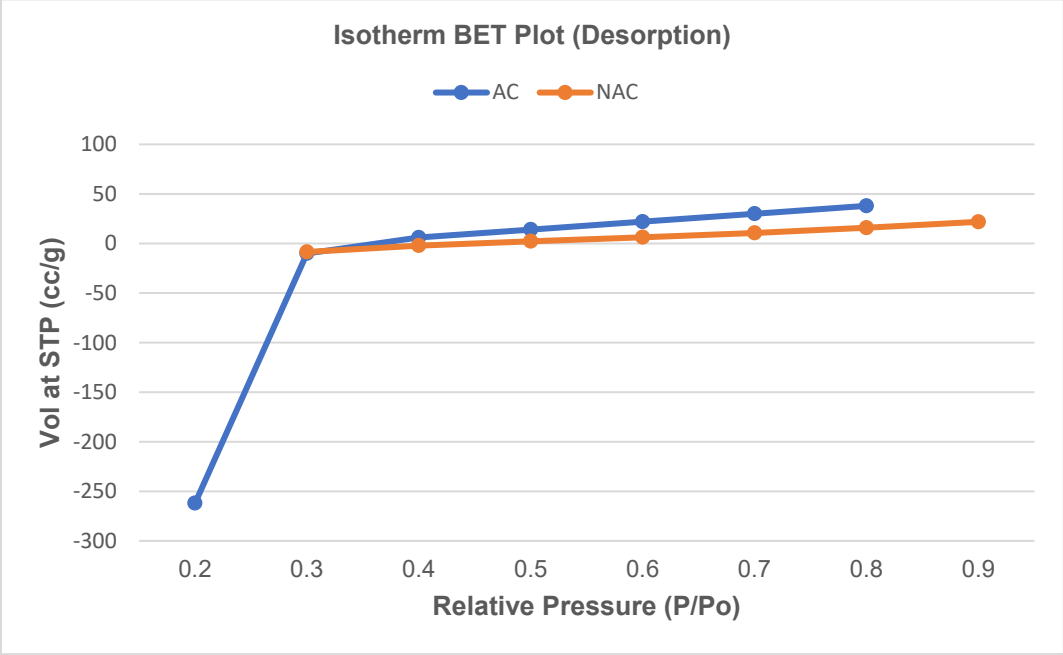

Fig. 10. Isotherm BET plot (desorption) of activated and nano-activated carbon

CONCLUSIONS

1. Dabai (*C. odontophyllum*) is a sustainable material that can create useful mixture material for adsorption applications. The presence of functional groups such as hydroxyl, phenolic, amide groups, and carbonyl on its surface provides strong adsorbent properties. The developed FTIR spectra revealed the presence of carboxylic compounds in the activated carbon sample, which improved its adsorption properties.
2. Apart from good adsorbent properties, biodegradable material can also reduce solid waste production once it has reached its lifespan. According to the findings, one of the crucial factors that influence the pore structure, adsorption capacity, and formation of active sites on mixture surfaces is the composition of mixture.
3. The findings of this study demonstrated that activated carbon derived from Dabai has a high potential for wastewater treatment. The characterization analyses revealed that both the non-activated and AC samples had an irregular, granular, and porous structure.
4. The pore dimension of AC is smaller than that of the non-activated carbon due to the blocking effect of metallic alkaline on the carbon matrix. The EDX analysis confirmed that carbonized materials have a higher percentage of carbon as the organic materials in the biomass decompose, resulting in a carbon-rich product. The specific surface area for nano activated carbon was higher than that of the activated carbon.

ACKNOWLEDGMENTS

The authors would like to express their most sincere appreciation and deepest gratitude to the Department of Chemical Engineering and Energy Sustainability, Faculty of Engineering, Universiti Malaysia, Sarawak.

REFERENCES CITED

Ahmad, A., and Azam, T. (2019) "Water purification technologies," in: *Bottled and Packaged Water*, A. M. Grumuezescu and A. M. Holban (eds.), Woodhead Publishing, 83-120. DOI: 10.1016/B978-0-12-815272-0.00004-0

Ahrouch, M., Gatica, J. M., Draoui, K., and Vidal, H. (2019). "Adding value to natural clays as low-cost adsorbents of methylene blue in polluted water through honeycomb monoliths manufacture," *SN Applied Sciences* 1(12), 1595. DOI: 10.1007/s42452-019-1636-4

Amador, C., and Martin, L. (2016). "Strategies for structured particulate systems design," in: *Computer Aided Chemical Engineering* 39, 509-579. DOI: 10.1016/B978-0-444-63683-6.00019-8

Arjmandi, R., Hassan, A., Haafiz, M. K. M., and Zakaria, Z. (2016). "Effects of micro- and nano-cellulose on tensile and morphological properties of montmorillonite nanoclay reinforced polylactic acid nanocomposites," in: *Nanoclay Reinforced Polymer Composites*, J. Mohammad, A. K. Qaiss, and R. Bouhfid (eds.) Springer, Singapore, Republic of Singapore.

ASTM E1252-98 (2021). "Standard practice for general techniques for obtaining infrared

spectra for qualitative analysis," ASTM International, West Conshohocken, PA.
ASTM E168-16 (2016). "Standard practices for general techniques of infrared quantitative analysis," ASTM International, West Conshohocken, PA.
ASTM E2015-04 (2014). "Standard guide for preparation of plastics and polymeric specimens for microstructural examination," ASTM International, West Conshohocken, PA.
Bernal, V., Giraldo, L., and Moreno-Piraján, J. C. (2018). "Physicochemical properties of activated carbon: Their effect on the adsorption of pharmaceutical compounds adsorbate-adsorbent interactions," *J. Carbon Res.* 4(4), 62. DOI: 10.3390/c4040062
Chen, S., Tang, S., Sun, Y., and Gang, W. (2018). "Preparation of a highly porous carbon material based on quinoa husk and its application for removal of dyes by adsorption," *Materials* 11(8), article no. 1407. DOI: 10.3390/ma11081407
Chikri, R., Elhadiri, N., Benchanaa, M., and El maguana, Y. (2020). "Efficiency of sawdust as low-cost adsorbent for dye removal," *Journal of Chemistry* 2020(8813420), 1-17. DOI: 10.1155/2020/8813420
Chobchun, M., Jutakridsada, P., Thiamsinsangwon, P., Kasemsiri, P., Kamwilaisak, K., and Chindaprasirt, P. (2020). "Characterization of TiO_2-activated carbon onto adsorption and photocatalytic properties and its application," *Journal of Metals, Materials and Minerals* 30(4), 30-38. DOI: 10.14456/jmmm.2020.48
Chowdhury, Z. Z., Hamid, S. B. A., Das, R., Hasan, R., Zain, S. M., Khalid, K., and Uddin, N. (2013). "Preparation of carbonaceous adsorbents from lignocellulosic biomass and their use in removal of contaminants from aqueous solution," *BioResources* 8(4), 6523-6555. DOI: 10.15376/biores.8.4.6523-6555
Darmawan, S., Wistara, N. J., Pari, G., Maddu, A., and Syafii, W. (2016). "Characterization of lignocellulosic biomass as raw material for the production of porous carbon-based materials," *BioResources* 11(2), 3561-3574. DOI: 10.15376/biores.11.2.3561-3574
Deng, J., Xiong, T., Wang, H., Zheng, A., and Wang, Y. (2016). "Effects of cellulose, hemicellulose, and lignin on the structure and morphology of porous carbons," *ACS Sustainable Chemistry & Engineering* 4(7), 3750-3756. DOI: 10.1021/acssuschemeng.6b00388
Djellabi, R., Yang, B., Wang, Y., Cui, X., and Zhao, X. (2019). "Carbonaceous biomass-titania composites with Ti-O-C bonding bridge for efficient photocatalytic reduction of Cr(VI) under narrow visible light," *Chemical Engineering Journal* 366, 172-180. DOI: 10.1016/j.cej.2019.02.035
Feng, P., Li, J., Wang, H., and Xu, Z. (2020). "Biomass-based activated carbon and activators: Preparation of activated carbon from corncob by chemical activation with biomass pyrolysis liquids," *ACS Omega* 5(37), 24064-24072. DOI: 10.1021/acsomega.0c03494
Gao, Y., Yue, Q., Gao, B., and Li, A. (2020). "Insight into activated carbon from different kinds of chemical activating agents: A review," *Science of The Total Environment* 746, 141094. DOI: 10.1016/j.scitotenv.2020.141094
Gisi, S. D., Lofrano, G., Grassi, M., and Notarnicola, M. (2016). "Characteristics and adsorption capacities of low-cost sorbents from wastewater treatment: A review," *Sustainable Mater. Technol.* 9, 10-40. DOI: 10.1016/j.susmat.2016.06.002
Heidarinejad, Z., Dehghani, M. H., Heidari, M., Javedan, G., Ali, I., and Sillanpää, M. (2020). "Methods for preparation and activation of activated carbon: A review," *Environmental Chemistry Letters* 18, 393-415. DOI: 10.1007/s10311-019-00955-0

Inderan, V., Sinnakaudan, S., Wahab, N. A. A., and Isa, N. (2014). "Preparation and characterisation of phosphoric acid activated carbon from *Canarium Odontophyllum (Dabai)* nutshell for methylene blue adsorption," *Research Journal of Chemistry and Environment* 18(2), 57-62.

Janusz, G., Pawlik, A., Sulej, J., Świderska-Burek, U., Jarosz-Wilkołazka, A., and Paszcyński, A. (2017). "Lignin degradation: Microorganisms, enzymes involved, genomes analysis and evolution," *FEM Microbiology Reviews* 41(6), 941-962. DOI: 10.1093/femsre/fux049

Kamil, F. Z. M., Hasanuddin, N. I., Othman, R., and Anuar, F. (2020). "Treatment of palm oil mill effluent by poly(L-lactic acid)-poly (ethylene glycol)/ silica membrane," *Sains Malaysiana* 49(9), 2311-2322. DOI: 10.17576/jsm-2020-4909-28

Karinkanta, P., Ämmälä, A., Illikainen, M., and Niinimäki, J. (2018). "Fine grinding of wood – Overview from wood breakage to applications," *Biomass and Bioenergy* 113, 31-44. DOI: 10.1016/j.biombioe.2018.03.007

Karoui, S., Arfi, R. B., Mougin, K., Ghorbal, A., Assadi, A. A., and Amrane, A. (2019). "Synthesis of novel biocomposite powder for simultaneous removal of hazardous ciprofloxacin and methylene blue: Central composite design, kinetic and isotherm studies using Brouers-Sotolongo family models," *Journal of Hazardous Materials* 387, 121675. DOI: 10.1016/j.jhazmat.2019.121675

Keane, D. (2013). *Evaluation of the Performance of Activated Carbon and Titanium Dioxide Composites for Pharmaceutical Adsorption and Photocatalysis in Water*, Ph.D. Dissertation, Dublin City University, Dublin, Ireland.

Khairulzaim, A. A. M., Rahman, M. R., Roslana, L., Bakri, M. K., Khan, A., and Matin, M. M. (2021). "Analysis of char prepared by pyrolysisof *Dabai (Canarium Odontophyllum)* nutshells as a potential precursor of biocarbon used for wastewater treatment," *BioResources* 16(3), 5036-5046. DOI: 10.15376/biores.16.3.5036-5046

Khui, P. L. N., Rahman, M. R, Hamdan, S., Jayamani, E., Bakri, M. K., and Sanaulla, K. (2020). "Synthesis and characterisation of micro-nano carbon filler from Jatropha seeds," *BioResources* 15(2), 3237-3251.

Kuang, Y., Zhang, X., and Shaoqi, Z. (2020). "Adsorption of methylene blue in water onto activated carbon by surfactant modification," *Water* 12(2), 587. DOI: 10.3390/w12020587

Kusiak-Nejman, E., Moszyński, D., Kapica-Kozar, J., Wanag, A., and Morawski, A. W. (2018). "Assessment of the suitability of the one-step hydrothermal method for preparation of non-covalently/covalently-bonded TiO_2/graphene-based hybrids," *Nanomaterials* 8(9), 647. DOI: 10.3390/nano8090647

Li, M., and Wilkins, M. (2020). "Lignin bioconversion into valuable products: Fractionation, depolymerization, aromatic compound conversion, and bioproduct formation," *Systems Microbiology and Biomanufacturing* 1(2), 166-185. DOI: 10.1007/s43393-020-00016-6

Li, X., Zhou, X., Shi, C., Xu, J., Li, Y., Tang, S., Huang, K., and Wang, X. (2016). "Preparation of a long-alkyl-chain silane grafted organic montmorillonite and its nanocomposites with SEBS," *Polymer Bulletin* 74(1), 107-120. DOI: 10.1007/s00289-016-1701-8

Maguana, Y. E., Elhadiri, N., Bouchdoug, M., Benchanaa, M., and Jaouad, A. (2019). "Activated carbon from prickly pear seed cake: Optimization of preparation conditions using experimental design and its application in dye removal," *Int. Journal of Chemical Engineering* 2019(8621951), 1-12. DOI: 10.1155/2019/8621951

Matteis, V. D., Cannavale, A., and Ayr, U. (2020). "Titanium dioxide in chromogenic devices: Synthesis, toxicological issues, and fabrication methods," *Applied Sciences* 10(24), 8896-8929. DOI: 10.3390/app10248896

Mistar, E. M., Alfatah, T., and Supardan, M. D. (2020). "Synthesis and characterization of activated carbon from *Bambusa vulgaris striata* using two-step KOH activation," *Journal of Materials Research and Technology* 9(3), 6278-6286. DOI: 10.1016/j.jmrt.2020.03.041

Min, H. S., Abbas, M., Kanthasamy, R., Aziz, H. A., and Chay, T. C. (2017). *Activated Carbon Prepared from Various Precursors*, Ideal Internat. E-Publ., Indore, India.

Mohammed, Z., Tcherbi-Narteh, A., and Jeelani, S. (2020). "Effect of graphene nanoplatelets and montmorillonite nanoclay on mechanical and thermal properties of polymer nanocomposites and carbon fiber reinforced composites," *SN Applied Sciences* 2(12), 1959. DOI: 10.1007/s42452-020-03780-1

Mu'aza, N. D., Jarrah, N., Zubair, M., and Alagha, O. (2017). "Removal of phenolic compounds from water using sewage sludge-based activated carbon adsorption: A review," *International Journal of Environmental Research and Public Health* 14(10), 1094. DOI: 10.3390/ijerph14101094

Murugadoss, S., Brassinne, F., Sebaihi, N., Petry, J., Cokic, S. M., Van Landuyt, K. L., Godderis, L., Mast, J., Lison, D., Hoet, P. H., *et al.* (2020). "Agglomeration of titanium dioxide nanoparticles increase toxicological responses in vitro and in vivo," *Particle and Fibre Toxicology* 17(1), 10. DOI: 10.1186/s12989-020-00341-7

Phanthong, P., Reubroycharoen, P., Hao, X., Xu, G., Abudula, A., and Guan, G. (2018). "Nanocellulose: Extraction and application," *Carbon Resources Conversion* 1(1), 32-43. DOI: 10.1016/j.crcon.2018.05.004

Poursorkhabi, V., Abdelwahab, M. A., Misra, M., Khalil, H., Gharabaghi, B., and Mohanty, A. K. (2020). "Processing, carbonization, and characterization of lignin based electrospun carbon fibers: A review," *Frontiers in Energy Research* 8, 208. DOI: 10.3389/fenrg.2020.00208

Quan, C., Su, R., and Gao, N. (2019). "Preparation of activated biomass carbon from pine sawdust for supercapacitor and CO_2 capture," *International Journal of Energy Research* 44(6), 4335-4351. DOI: 10.1002/er.5206

Saleem, J., Shahid U.B., Hijab, M., Mackey, H., McKay, G. (2019). "Production and applications of activated carbons as adsorbents from olive stones," *Biomass Conversion and Biorefinery* 9(1), 775-802. DOI: 10.1007/s13399-019-00473-7

Salim, R. M., Asik, J., and Sarjadi, M. S. (2021). "Chemical functional groups of extractives, cellulose and lignin extracted from native *Leucaena leucocephala* bark," *Wood Science and Technology* 55, 295-313. DOI: 10.1007/s00226-020-01258-2

Son, B. T., Long, N. V., and Hang, N. T. N. (2021). "The development of biomass-derived carbon-based photocatalysts for the visible-light-driven photodegradation of pollutants: A comprehensive review," *RSC Advances* 49(11), 30574-30596. DOI: 10.1039/D1RA05079F

Srivatsav, P., Bhargav, B. S., Shanmugasundaram, V., Arun, J., Gopinath, K. P., and Bhatnagar, A. (2020). "Biochar as an eco-friendly and economical adsorbent for the removal of colorants (dyes) from aqueous environment: A review," *Water* 12(12), 3561. DOI: 10.3390/w12123561

Taoufik, N., Elmchaouri, A., Anouar, F., Korili, S., and Gil, A. (2019) "Improvement of the adsorption properties of an activated carbon coated by titanium dioxide for the removal of emerging contaminants," *Journal of Water Process Engineering* 31,

100876. DOI: 10.1016/j.jwpe.2019.100876

Yang, H. M., Zhang, D. H., Chen, Y., Ran, M. J., and Gu, J. C. (2017). "Study on the application of KOH to produce activated carbon to realize the utilization of distiller's grains," *IOP Conference Series: Earth and Environmental Science* 69, 012051. DOI: 10.1088/1755-1315/69/1/012051

Varma, R. S. (2019). "Biomass-derived renewable carbonaceous materials for sustainable chemical and environmental applications," *ACS Sustainable Chemistry Engineering* 7(7), 6458-6470. DOI: 10.1021/acssuschemeng.8b06550

Wataniyakul, P., Boonnoun, P., Quitain, A. T., Sasaki, M., Kida, T., Laosiripojana, N., and Shotipruk, A. (2018). "Preparation of hydrothermal carbon as catalyst support for conversion of biomass to 5-hydroxymethylfurfural," *Catalysis Communications* 104, 41-47. DOI: 10.1016/j.catcom.2017.10.014

Zaman, C. Z., Pal, K., Yehye, W. A., Sagadevan, S., Shah, S. T., Adebisi, G. A., Marliana, E., Rafique, R. F., and Johan, R. B. (2017). "Pyrolysis: A sustainable way to generate energy from waste," in: *Pyrolysis*, M. Samer (ed.) IntechOpen, London, UK.

Zhang, Q., Wang, J., Lyu, H., Zhao, Q., Jiang, L., and Liu, L. (2019). "Ball-milled biochar for galaxolide removal: Sorption performance and governing mechanisms," *Sci. Total Environ.* 659, 1537-1545. DOI: 10.1016/j.scitotenv.2019.01.005

Zheng, Y., Fu, Z., Li, D., and Wu, M. (2018). "Effects of ball milling processes on the microstructure and rheological properties of microcrystalline cellulose as a sustainable polymer additive," *Materials* 11(7), 1057. DOI: 10.3390/ma11071057

Zuo, W., Shi, B., Chen, S., Zhou, X., Duan, Y., and Liao, A. (2018). "Low-cost and efficient adsorbent derived from pyrolysis of *Jatropha curcas* seeds for the removal of Cu^{2+} from aqueous solutions," *Chem. Ecol.* 34(7), 655-674. DOI: 10.1080/02757540.2018.1472246

Article submitted: Dec. 23, 2021; Peer review completed: April 16, 2022; Revised version received: May 22, 2022; Accepted after further revisions: May 27, 2022; Published: June 3, 2022.
DOI: 10.15376/biores.17.3.4452-4469